PCCP

Accepted Manuscript

ROYAL SOCIETY OF CHEMISTRY

www.rsc.org/pccp

Physical Chemistry Chemical Physics
CREATED USING THE RSC LaTeX PCCP ARTICLE TEMPLATE – SEE www.rsc.org/electronicfiles FOR DETAILS
ARTICLE TYPE www. rsc.org/xxxxxx | XXXXXXXX

From semiconductor nanocrystals to artificial solids with dimensionality below two

Christophe Delerue[*a]

Received Xth XXXXXXXXXX 20XX, Accepted Xth XXXXXXXXX 20XX
First published on the web Xth XXXXXXXXXX 200X
DOI: 10.1039/b000000x

Two-dimensional films of semiconductors can be patterned into super-lattices with a nanoscale periodicity, using top-down (lithography) or bottom-up approaches. In particular, square and honeycomb lattices of semiconductor nanocrystals have been recently synthesized using oriented attachment. We have performed atomistic tight-binding calculations of the conduction bands of super-lattices of CdSe. We consider spherical nanocrystals connected by horizontal cylinders and we investigate the band structure between two extreme limits, the uniform two-dimensional film, and the assembly of disconnected nanocrystals. Using this model system, we explain how rich band structures emerge from the periodic nano-geometry, including Dirac cones and non-trivial flat bands in honeycomb lattices. The possibility to build non-conventional band structures using multi-orbital artificial atoms (nanocrystals) opens up new prospects.

1 Introduction

Two-dimensional (2D) semiconductors grown for example by molecular beam epitaxy are widely employed to fabricate diode lasers, High Electron Mobility Transistors (HEMT) or photo-detectors.[1] In addition, the 2D electron gases which can be formed in these structures exhibit very interesting physical properties[2,3] like the quantum Hall effect.[4] Recently, the interest for 2D materials has been considerably renewed thanks to the discovery of graphene[5] which motivated research in different directions, for example on silicene[6] and MoS_2.[7] Graphene and silicene have a honeycomb lattice and therefore present in their band structure very interesting features like Dirac cones which have no counterpart in usual 2D semiconductors. Inspired by these discoveries, it was proposed to impose a honeycomb pattern on a 2D semiconductor by using lithography or arrays of metallic gates as, in analogy with graphene,[8–11] linear $E(\vec{k})$ relationships were predicted close to the K points in the Brillouin zone.

Band engineering of 2D semiconductor materials is also thinkable following a bottom-up approach since the building blocks are already available in the form of semiconductor nanocrystal (NC) quantum dots. Semiconductor NCs are characterized by discrete energy levels close to their bandgap. It is therefore tempting to assemble these artificial atoms to fabricate new materials with non-conventional properties. As a matter of fact, NC solids obtained by self-assembly have been reported many times.[12–18] However, the NCs in these assemblies are separated by an organic or inorganic barrier, resulting in a weak coupling between the NCs which prevents the formation of true electronic bands. A real breakthrough in the field came from the discovery of the oriented attachment of NCs[19–25] which produces atomically-coherent semiconductor nanostructures which can be lead, in the best cases, to single-crystalline super-lattices. Remarkably, square[24,25] and honeycomb[24] lattices of PbSe NCs have been recently synthesized by this technique and their transformation into super-lattices of CdSe NCs by a Cd-for-Pb cation exchange has been demonstrated.[24] Calculations that we have performed recently for square[26] and honeycomb[27] lattices of (PbSe) CdSe NCs predict band structures which strongly deviate from that of genuine 2D semiconductors.

Thus, we are in a situation where top-down and bottom-up approaches are available to produce semiconductor super-lattices in which the dimensionality can be varied from 2D (uniform sheets) to 0D (arrays of weakly coupled NCs). Our objective in this paper is to explore fundamentally the evolution of the band structure between these two limits. In Refs. 26,27, we investigated lattices formed by the oriented attachment along $\langle 100 \rangle$ (square) or $\langle 110 \rangle$ (honeycomb) facets of NCs in the shape of truncated nanocubes. However, the exact shape of the NCs after oriented attachment and cation exchange is not exactly known. In situ Transmission Electron Microscopy (TEM) experiments[28] and atomistic simulations[29] show that important atomic reorganization takes place during the attachment process. Therefore, in this paper, we consider square and honeycomb lattices with another structure consisting of spherical NCs connected by horizontal cylinders. Such a geometry can be seen not only as a model system but also is compatible with TEM observations of the lattices after

[a] *IEMN - Dept. ISEN, UMR CNRS 8520, Lille, France; Tel: +33 3 20 30 40 53; E-mail: christophe.delerue@isen.fr*

cation exchange.[24] Another interest of this geometry is that we can tune the electronic structure continuously between two extreme limits, the isolated NCs and the uniform 2D film, allowing to interpret its evolution in a simple manner. We will show that patterning 2D semiconductors into square or honeycomb super-lattices leads to non-conventional band structures, beyond what was anticipated in early works.[8–11] In particular, we will understand how Dirac cones and non-trivial flat bands can be formed under the honeycomb nano-geometry.[27] In the following, we focus our study on the conduction bands of CdSe super-lattices which exhibit a very rich behaviour, far from the simple isotropic conduction band of bulk CdSe.

2 Methodology

The band structure of square and honeycomb super-lattices of CdSe is explored through atomistic tight-binding calculations. In accordance with experimental observations,[24] the atoms inside the NCs and the cylinders are positioned at the same atomic sites as in bulk zinc-blende CdSe. Each atom is described by a double set of $sp^3d^5s^*$ atomic orbitals including the spin degree of freedom. The orbitals are assumed to be orthogonal and the matrix elements between two orbitals are restricted to first nearest-neighbor interactions. The Hamiltonian is written as a function of parameters (given in Ref. 26) which are adjusted in order to get the best band structure for bulk CdSe compared to *ab initio* calculations and experimental data.[26] There is no free parameter in the calculations. Spin-orbit coupling is included even if its influence is weak in the conduction band of CdSe. Surfaces are saturated by pseudo-hydrogen atoms to avoid gap states induced by surface dangling bonds. Due to the large size of the systems that we have considered (up to 10^4 atoms per unit cell), the numerical methods described in Ref. 30 are used to calculate near-gap states. Throughout the paper, the zero of energy corresponds to the top of the valence band of bulk CdSe.

Self-energy corrections are known to provide noticeable corrections to band structures of semiconductors.[31–33] In bulk, they mainly result in a rigid shift of conduction bands with respect to valence bands. This effect is implicitly included in our tight-binding parameters fitted on the experimental bandgap. In quantum confined systems, additional size-dependent self-energy corrections must be considered[32,33] but, once again, they mainly induce a rigid shift of empty levels with respect to occupied ones.[33,34] Therefore, in the present work, since we are not interested in the absolute position of the conduction bands of the super-lattices, self-energy corrections are neglected. Similarly, optical properties (and therefore excitonic effects) are not considered here.

3 Square lattices

We consider square lattices built from spherical NCs of diameter D (Fig. 1a). We set the centre-to-centre distance a between nearest-neighbour NCs equal to D, i.e., the spheres are tangential. Between each pair of neighbours, we add a cylinder of atoms that serves as a bond. The cylinders are oriented along $\langle 100 \rangle$ crystallographic directions. All Cd and Se atoms contained in the spheres and the cylinders are included in the structure. Depending on the size, it results in slightly facetted shapes (Fig. 1b). When we change the cylinder diameter d from 0 to D, we will see that we vary considerably the coupling between NCs. The number (N_{at}) of atoms in a plane perpendicular to a cylinder is approximately equal to $4.3d^2$ where d is in nanometer.

Typical conduction band structures are presented in Fig. 1e-g. They are composed of successive mini-bands, a quite general behaviour in super-lattices, for example made by the successive growth of thin semiconductor wells and barriers.[3] However, we will see that the nanoscale patterning offers much more possibilities of band engineering.

In order to interpret these results, it is worth considering the super-lattices as though they were obtained by a top-down approach, starting from bulk CdSe characterized by an isotropic conduction band (red dotted line in Fig. 1c). We first form a 2D film and, second, a super-lattice. In a uniform film of CdSe, the quantum confinement along one dimension leads to the formation of subbands whose dispersion is presented in the extended zone scheme in Fig. 1c. When a square super-lattice is created from the 2D film, the first effect which must be taken into account is the increased size of the super-cell. We have therefore redrawn the band structure of the uniform film in the restricted zone scheme (Fig. 1d), by folding the bands into the Brillouin zone (inset of Fig. 1g) of the super-lattice. The second effect comes from the potential induced by the formation of holes in the super-lattice which scatter periodically the electronic waves. It opens gaps in particular at the centre and at the edges of the Brillouin zone, exactly like when we consider quasi-free electron bands starting from free electron ones.[33,35] This is exactly the behaviour that we predict for $d/D = 1$ (Fig. 1e), i.e., when there are periodic holes in the layer but the bonds between neighbour NCs are strong. When d/D is reduced (Fig. 1f), the effect of the scattering potential increases and the bands strongly deviate from the 2D film case. In particular, absolute gaps appear, separating a lowest band and a set of three bands from the higher-energy bands (all the bands are spin-degenerate). In addition, all the bands shift to higher energy due to the stronger quantum confinement when the holes are created. Finally, when $d/D \to 0$, the coupling between NCs becomes vanishingly small and the bands collapse at the energy levels of the individual NCs (Fig. 1g).

It is also instructive to discuss the results from a bottom-

up perspective, i.e., starting from the limit of individual NCs ($d/D = 0.1$, Fig. 1g). Due to the strong confinement in the three directions of space, each NC is characterized by discrete levels, a spin-degenerate electron state with a $1S$ envelope wave function as a ground state, and three spin-degenerate $1P$ excited states higher in energy. By increasing slightly the value of d/D, the lowest manifolds of bands arise from the coupling between the $1S$ and $1P$ states of neighbour NCs, respectively (Fig. 1f). In the limit where the coupling $V_{ss\sigma}$ (notations of Ref. 36) between neighbour $1S$ states is small compared to the $1S-1P$ splitting, the $1S$ band can be described by an effective model of s orbitals on a square lattice. In this effective model, the $1S$ band energy is given by

$$E_s(\vec{k}) = E_s + 2V_{ss\sigma}\left[\cos(k_x a) + \cos(k_y a)\right] \quad (1)$$

where E_s is the onsite $1S$ energy (xOy is the lattice plane). The energy dispersion of the $1P$ bands can be calculated similarly if we consider σ ($V_{pp\sigma}$) and π ($V_{pp\pi}$) interactions between neighbour $1P$ states. Taking into account that the problem for the $1P_x$, $1P_y$ and $1P_z$ bands can be decoupled, we get

$$\begin{aligned} E_x(\vec{k}) &= E_{p_x} + 2V_{pp\sigma}\cos(k_x a) + 2V_{pp\pi}\cos(k_y a) \\ E_y(\vec{k}) &= E_{p_x} + 2V_{pp\sigma}\cos(k_y a) + 2V_{pp\pi}\cos(k_x a) \\ E_z(\vec{k}) &= E_{p_z} + 2V_{pp\pi}\left[\cos(k_x a) + \cos(k_y a)\right] \end{aligned} \quad (2)$$

where E_{p_x} (E_{p_z}) is the onsite $1P_x$ ($1P_z$) energy (by symmetry, $E_{p_x} = E_{p_y}$). The $1S$ and $1P$ bands in Fig. 1f are well described by Eqns. 1 and 2. The π coupling is much smaller than the σ coupling, explaining why the $1P_z$ band is basically flat. Higher energy bands shown in Fig. 1f originate from $1D$ and $2S$ states of the NCs.

When the coupling (i.e., d/D) between neighbour NCs is increased (Fig. 1e), the width of the bands increases as well as the hybridization between $1S$ and $1P$ states (or $1P$ and $1D$). As already discussed above, when $d/D \to 1$, we recover a situation close to the uniform 2D case. Between the extreme limits, the dimensionality of the super-lattices can be referred to as being below two, since the electrons move on a 2D lattice but their properties are governed by the confinement on each site which can be seen as a multi-orbital atom.

4 Honeycomb lattices

We consider honeycomb lattices built similarly from tangential spherical NCs connected by cylinders (Fig. 2a). The cylinders are along $\langle 110\rangle$ crystallographic directions ($N_{at} \approx 6.0d^2$). For d of the order of 20-50% of D, we predict conduction band structures very close to those obtained with truncated nanocubes.[27] There are two well-separated manifolds of two and six bands (4 and 12 bands including spin). The lowest bands have the same type of dispersion as the π and π^* bands in real graphene,[5,37] in particular Dirac cones are present at the K and K' points of the Brillouin zone. In the second manifold higher in energy, four bands have a small dispersion and two others form very dispersive Dirac bands. The great similarity of these results with those obtained for honeycomb lattices of truncated nanocubes show that the exact shape of the NCs is not a main factor determining the formation of band structures with the same behaviour.

In order to understand the origin of these bands, it is once again instructive to compare with the case where d/D is very small, i.e. when the coupling between nearest-neighbour NCs becomes negligible. As expected, Fig. 2b shows that all the bands are totally flat for $d/D \approx 0.1$ ($D = 4.7$ nm), they are positioned at the energy levels of the individual NCs. By increasing slightly the value of d/D, we see that the two manifolds of bands in the honeycomb super-lattice arise from the coupling between these $1S$ and $1P$ states of neighbour NCs, respectively (Fig. 2c).

The bands in these systems are formed exactly like in graphene except that the carbon atoms are replaced by multi-orbital artificial atoms, the NCs. When the coupling between nearest-neighbour NCs is weak (compared to the splitting between discrete states), the effective Hamiltonian restricted to the $1S$ orbitals is formally the same as for p_z orbitals in graphene,[5,37] explaining why we recover $1S$ bands with exactly the same behaviour as $\pi-\pi^*$ bands of graphene but with renormalized hopping term:[27]

$$\begin{aligned} E_s(\vec{k}) &= E_s \pm V_{ss\sigma} \\ &\times \sqrt{3 + 2\cos(\sqrt{3}k_y a) + 4\cos\left(\frac{\sqrt{3}}{2}k_y a\right)\cos\left(\frac{3}{2}k_x a\right)} \end{aligned} \quad (3)$$

The dispersion at the K and K' points is linear (Dirac points) as imposed by the honeycomb nano-geometry.[5,37] Like in the case of square lattices, Fig. 2 shows that the width of each band is directly linked to the strength of the bond joining each neighbour NC. Remarkably, for d/D of the order of 0.5 and above, bandwidths above 100 meV are obtained. Interestingly, with this nanoscale geometry, the $1S$ and $1P$ bands never overlap, even for $d/D = 1$. However, for high values of d/D, the shape of the bands is strongly deformed due to the coupling between $1S$ and $1P$ states. For example, as it could be easily shown by perturbation theory, the effect of the $S-P$ coupling within the $1S$ manifold can be effectively described by a second-nearest-neighbour coupling term between $1S$ orbitals. This kind of term is known to induce asymmetry between the π and π^* bands of graphene.[5] The same effect is clearly visible in our artificial graphene (Fig. 2f).

When the coupling is not too strong, the behaviour of the $1P$ bands can be described by a model of electrons moving

on a honeycomb lattice with three p orbitals on each site.[38,39] As shown in the inset of Fig. 2d, the coupling between $1P_{x,y}$ orbitals leads to the formation of four bands: two dispersive bands with Dirac cones at K and K, and two flat bands, respectively above and below the Dirac bands. These bands are flat due to destructive interferences of electron hopping induced by the honeycomb nano-geometry (non-trivial flat band).[38,39] The $1P_z$ states, oriented perpendicularly to the lattice, are weakly coupled by π-like interactions ($V_{pp\pi} \approx 0$) and give rise to two flattened bands (trivial flat band). When $V_{pp\pi}$ is neglected, the $1P$ bands are approximately described by an effective p-orbital Hamiltonian leading to[38]

$$\begin{aligned} E_z(\vec{k}) &\approx E_{p_z}, \\ E_{xy}^{(1)}(\vec{k}) &= E_{p_x} \pm \frac{3}{2} V_{pp\sigma}, \\ E_{xy}^{(2)}(\vec{k}) &= E_{p_x} \pm \frac{V_{pp\sigma}}{2} \sqrt{3 + 2\sum_i cos(\vec{k}\cdot\vec{e}_i)}, \end{aligned} \quad (4)$$

where $\vec{e}_1 = a\left(-\frac{\sqrt{3}}{2}, \frac{3}{2}\right)$, $\vec{e}_2 = a\left(-\frac{\sqrt{3}}{2}, -\frac{3}{2}\right)$, $\vec{e}_3 = a\left(\sqrt{3}, 0\right)$. $E_{xy}^{(1)}$ in the second line of Eq. 4 corresponds to the non-trivial flat bands. When the coupling between NCs increases, the higher $1P$ bands become more dispersive, in particular due to the hybridization with $1D$ like bands (higher bands are not shown). However, even for $d/D \approx 1$, the lowest flat band, below the $1P$ Dirac bands, remains non dispersive, protected by the topology.[38,39]

The conduction band structure of a uniform 2D film of CdSe is depicted in Fig. 2i. For the sake of comparison, we consider the same film thickness $D = 4.7$ nm, and the band structure is presented in the same Brillouin zone as for the honeycomb lattices. In order to see the effect of the nano-geometry on the bands, we have considered in Figs. 2g,h the same 2D film but in which we apply a repulsive potential on each atom that does not belong to the honeycomb lattice characterized by $d/D = 1$. By tuning this potential, we can describe continuously all the situations between the uniform film (Fig. 2i) and the honeycomb lattice (Fig. 2f). The repulsive potential induces periodic scattering of the electronic waves, opening gaps between the bands. Increasing the potential (Fig. 2g), the $1S$ band is separated from the others, the lowest flat band can be distinguished progressively.

5 Effective band structure parameters

The width of $1S$ and $1P$ bands is presented as a function of d/D in Fig. 3 for both types of lattices and for selected values of D. The gap between $1S$ and $1P$ bands is also shown. The bandwidths increase approximately linearly with d/D, except for $1P$ bands in honeycomb lattices where the bandwidth saturates for d/D above ~ 0.7 due to the coupling to higher-energy bands (e.g., $1D$ bands). Consequently, the $1S-1P$ gap decreases linearly with d/D. The bandwidths approximately vary as $\alpha(d/D-0.1)$ where α is a parameter that depends on D. From the fit on many configurations (D between 3 and 9 nm), it is found that α behaves as $1/D^2$. From Eqns. (1−4), the $1S$ and $1P$ bandwidths are equal to $|8V_{ss\sigma}|$ and $4V_{pp\sigma}$ for square lattices, and to $|6V_{ss\sigma}|$ and $3V_{pp\sigma}$ for honeycomb lattices, respectively (neglecting $V_{pp\pi}$). Remarkably, the values for $V_{ss\sigma}$ and $V_{pp\sigma}$ deduced for square and honeycomb lattices are very similar. We deduce general laws for the effective band structure parameters

$$V_{ss\sigma} \approx -26\left(\frac{5}{D}\right)^2\left(\frac{d}{D}-0.1\right), \quad (5)$$

$$V_{pp\sigma} \approx 107\left(\frac{5}{D}\right)^2\left(\frac{d}{D}-0.1\right), \quad (6)$$

in which D is in nanometer, $V_{ss\sigma}$ and $V_{pp\sigma}$ are in meV. Equations (5) and (6) are therefore valid for square and honeycomb lattices.

Figure 3c shows the variation with d/D of the effective mass m^* at Γ for the lowest $1S$ band of honeycomb lattices. m^* decreases with increasing d/D because the bands become more dispersive for stronger coupling between nearest-neighbour nanocrystals. m^* can be approximated by [Eqn. (3)]:

$$m^* = \frac{2\hbar^2}{3V_{ss\sigma}a^2}. \quad (7)$$

Similarly, the effective mass at Γ for the $1S$ band of square lattices is given by [Eqn. (1)]:

$$m^* = \frac{\hbar^2}{2V_{ss\sigma}a^2}. \quad (8)$$

Another interesting quantity that characterizes $1S$ bands for honeycomb lattices is the group velocity $v_g = \hbar^{-1}\partial E/\partial k$ at the Dirac point. Figure 3c shows that v_g increases with d/D and reaches quite high values, about 100 km/s or even higher, only one order of magnitude smaller than in graphene. v_g is approximately given by [Eqn. (3)]:[5]

$$v_g = \frac{3V_{ss\sigma}a}{2\hbar}. \quad (9)$$

In the case of graphene, the hopping parameter is about two orders of magnitude larger than $V_{ss\sigma}$ but the lattice parameter a is more than ten times smaller.[5]

Finally, it is important to emphasize that very similar results would be obtained for other semiconductors characterized by a single isotropic conduction band. We have checked that it is

the case for CdTe and InP. All the effective parameters (hopping terms, bandwidths, $1S-1P$ gap) basically scale as the inverse of the bulk effective mass. Therefore, the most interesting band structures will be obtained for semiconductors with a small effective mass. For semiconductors characterized by degenerate valleys such as PbSe (or Si), the mixing of the valleys plus the inter-valley couplings leads to more complex band dispersions.[27]

6 Conclusions

In conclusion, we have performed atomistic tight-binding calculations in order to understand the formation of the bands in planar super-lattices consisting of spherical NCs connected by horizontal cylinders. These systems are designed as models for super-lattices which can be fabricated either by top-down lithography or by bottom-up self-assembling of semiconductor NCs. We predict very rich band structures for materials in which the NCs behave as multi-orbital artificial atoms assembled on a lattice. Our theoretical study should motivate further works to explore the possibilities offered by these super-lattices with effective dimensionality below two.

References

1 C. Weisbuch and B. Vinter, *Quantum Semiconductor Structures: Fundamentals and Applications*, Academic Press, 1991.

2 T. Ando, A. B. Fowler and F. Stern, *Rev. Mod. Phys.*, 1982, **54**, 437–672.

3 G. Bastard, *Wave mechanics applied to semiconductor heterostructures*, Les Éditions de Physique, 1988.

4 K. v. Klitzing, G. Dorda and M. Pepper, *Phys. Rev. Lett.*, 1980, **45**, 494–497.

5 A. H. Castro Neto, F. Guinea, N. M. R. Peres, K. S. Novoselov and A. K. Geim, *Rev. Mod. Phys.*, 2009, **81**, 109.

6 B. Lalmi, H. Oughaddou, H. Enriquez, A. Kara, S. Vizzini, B. Ealet and B. Aufray, *Appl. Phys. Lett.*, 2010, **97**, 223109.

7 K. F. Mak, C. Lee, J. Hone, J. Shan and T. F. Heinz, *Phys. Rev. Lett.*, 2010, **105**, 136805.

8 C.-H. Park and S. G. Louie, *Nano Lett.*, 2009, **9**, 1793–1797.

9 G. D. Simoni, A. Singha, M. Gibertini, B. Karmakar, M. Polini, V. Piazza, L. N. Pfeiffer, K. W. West, F. Beltram and V. Pellegrini, *Appl. Phys. Lett.*, 2010, **97**, 132113.

10 M. Gibertini, A. Singha, V. Pellegrini, M. Polini, G. Vignale, A. Pinczuk, L. N. Pfeiffer and K. W. West, *Phys. Rev. B*, 2009, **79**, 241406.

11 L. Nádvorník, M. Orlita, N. A. Goncharuk, L. Smrčka, V. Novák, V. Jurka, K. Hruška, Z. Výborný, Z. R. Wasilewski, M. Potemski and K. Výborný, *New J. Phys.*, 2012, **14**, 053002.

12 D. Yu, C. Wang and P. Guyot-Sionnest, *Science*, 2003, **300**, 1277–1280.

13 D. Vanmaekelbergh and P. Liljeroth, *Chem. Soc. Rev.*, 2005, **34**, 299–312.

14 D. V. Talapin, J.-S. Lee, M. V. Kovalenko and E. V. Shevchenko, *Chem. Rev.*, 2010, **110**, 389–458.

15 M. V. Kovalenko, M. Scheele and D. V. Talapin, *Science*, 2009, **324**, 1417–1420.

16 E. Talgorn, R. D. Abellon, P. J. Kooyman, J. Piris, T. J. Savenije, A. Goossens, A. J. Houtepen and L. D. A. Siebbeles, *ACS Nano*, 2010, **4**, 1723–1731.

17 D. Steiner, D. Azulay, A. Aharoni, A. Salant, U. Banin and O. Millo, *Nanotechnology*, 2008, **19**, 065201.

18 D.-K. Ko, J. J. Urban and C. B. Murray, *Nano Lett.*, 2010, **10**, 1842–1847.

19 K.-S. Cho, D. V. Talapin, W. Gaschler and C. B. Murray, *J. Am. Chem. Soc.*, 2005, **127**, 7140–7147.

20 P. T. K. Chin, J. W. Stouwdam and R. A. J. Janssen, *Nano Lett.*, 2009, **9**, 745–750.

21 J. Zhang, F. Huang and Z. Lin, *Nanoscale*, 2010, **2**, 18–34.

22 C. Schliehe, B. H. Juarez, M. Pelletier, S. Jander, D. Greshnykh, M. Nagel, A. Meyer, S. Foerster, A. Kornowski, C. Klinke and H. Weller, *Science*, 2010, **329**, 550–553.

23 S. Ithurria and B. Dubertret, *J. Am. Chem. Soc.*, 2008, **130**, 16504–16505.

24 W. H. Evers, B. Goris, S. Bals, M. Casavola, J. de Graaf, R. van Roij, M. Dijkstra and D. Vanmaekelbergh, *Nano Lett.*, 2013, **13**, 2317–2323.

25 W. J. Baumgardner, K. Whitham and T. Hanrath, *Nano Lett.*, 2013, **13**, 3225–3231.

26 E. Kalesaki, W. H. Evers, G. Allan, D. Vanmaekelbergh and C. Delerue, *Phys. Rev. B*, 2013, **88**, 115431.

27 E. Kalesaki, C. Delerue, C. Morais Smith, W. Beugeling, G. Allan and D. Vanmaekelbergh, *Phys. Rev. X*, 2014, **4**, 011010.

28 M. A. van Huis, L. T. Kunneman, K. Overgaag, Q. Xu, G. Pandraud, H. W. Zandbergen and D. Vanmaekelbergh, *Nano Lett.*, 2008, **8**, 3959–3963.

29 P. Schapotschnikow, M. A. van Huis, H. W. Zandbergen, D. Vanmaekelbergh and T. J. H. Vlugt, *Nano Lett.*, 2010, **10**, 3966–3971.

30 Y. M. Niquet, C. Delerue, G. Allan and M. Lannoo, *Phys. Rev. B*, 2000, **62**, 5109–5116.

31 V. I. Gavrilenko and F. Bechstedt, *Phys. Rev. B*, 1997, **55**, 4343–4352.

32 G. Onida, L. Reining and A. Rubio, *Rev. Mod. Phys.*, 2002, **74**, 601–659.
33 C. Delerue and M. Lannoo, *Nanostructures: Theory and Modeling*, Springer, 2004.
34 C. Delerue, M. Lannoo and G. Allan, *Phys. Rev. Lett.*, 2000, **84**, 2457–2460.
35 W. A. Harrison, *Electronic Structure and the Properties of Solids: The Physics of the Chemical Bond*, Dover, 1989.
36 J. C. Slater and G. F. Koster, *Phys. Rev.*, 1954, **94**, 1498–1524.
37 P. R. Wallace, *Phys. Rev.*, 1947, **71**, 622–634.
38 C. Wu, D. Bergman, L. Balents and S. Das Sarma, *Phys. Rev. Lett.*, 2007, **99**, 070401.
39 K. Sun, Z. Gu, H. Katsura and S. Das Sarma, *Phys. Rev. Lett.*, 2011, **106**, 236803.

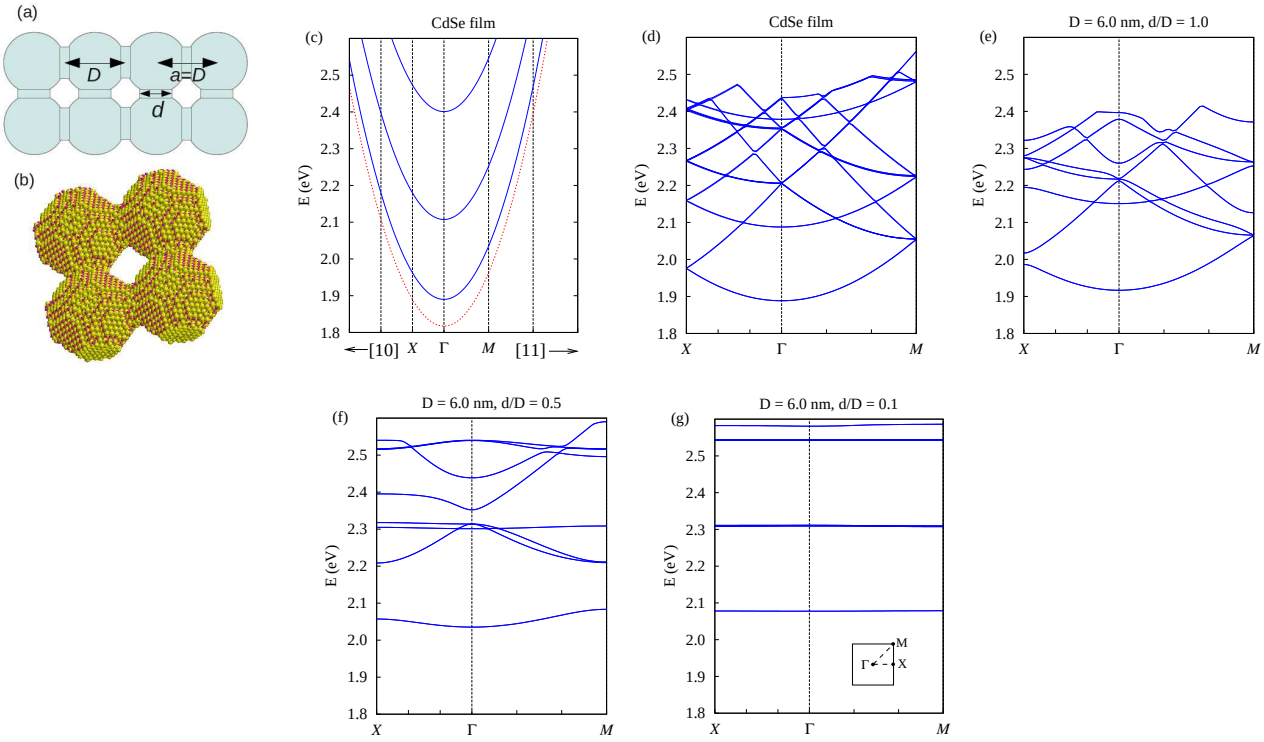

Fig. 1 (a) Schematic view of a square lattice of CdSe consisting of tangential spheres (diameter D = lattice spacing a) connected by horizontal cylinders (diameter d). (b) Atomistic view of four unit cells of the square lattice for $D = 6.0$ nm and $d/D = 0.5$. The yellow (red) spheres represent the Cd (Se) atoms. Pseudo-hydrogen atoms passivating the surface are not shown for clarity. (e-g) Lowest conduction bands calculated using the atomistic tight-binding method for $D = a = 6.0$ nm and varying ratio d/D. For clarity, only sixteen bands are shown. The Brillouin zone is shown as an inset in (g). (d) Conduction band structure of a 2D CdSe film (thickness = D) presented in the Brillouin zone of the square lattice for comparison (restricted zone scheme). (c) Same but represented in the extended zone scheme. The red dotted line corresponds to the conduction band of bulk CdSe.

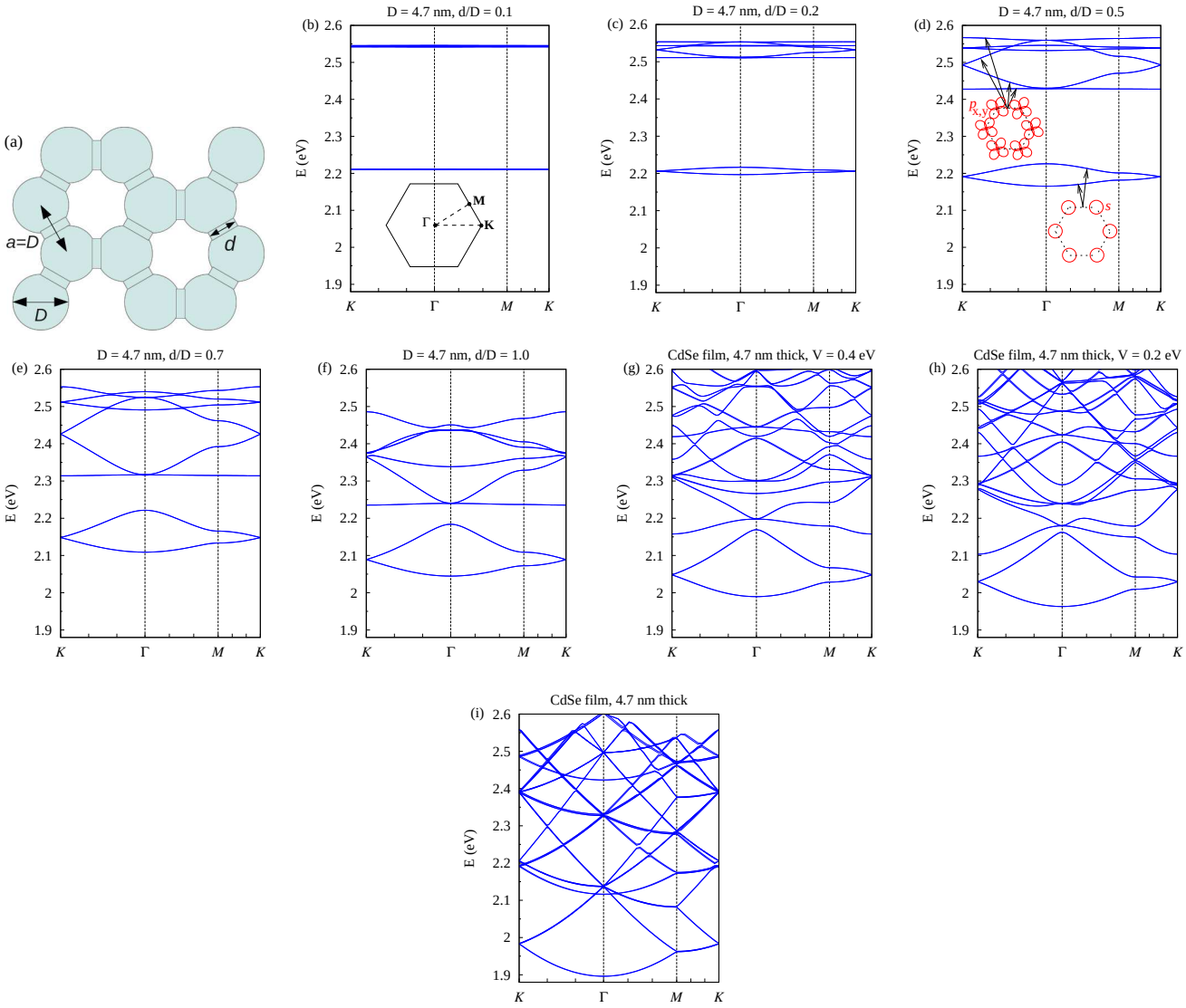

Fig. 2 (a) Honeycomb lattice of CdSe consisting of tangential spheres (diameter D = lattice spacing a) connected by horizontal cylinders (diameter d). (b-f) Lowest conduction bands calculated using the atomistic tight-binding method for $D = a = 4.7$ nm and varying ratio d/D. For clarity, only sixteen bands are shown. The inset in (b) depicts the Brillouin zone. The insets in (d) indicate the bands which mainly result from the coupling between $1S$ states, or between $1P_x$ and $1P_y$ states, respectively. (i) Conduction band structure of a 2D CdSe film (thickness = 4.7 nm) presented in the Brillouin zone of the honeycomb lattice for comparison. (g,h) Same but a repulsive potential V is applied on each atom of the film which does not belong to the honeycomb lattice characterized by $d/D = 1.0$ [$V = 0.4$ eV for (g), $V = 0.2$ eV for (h)]. These two figures show the transition from (f) to (i), i.e., from the honeycomb lattice to the 2D film.

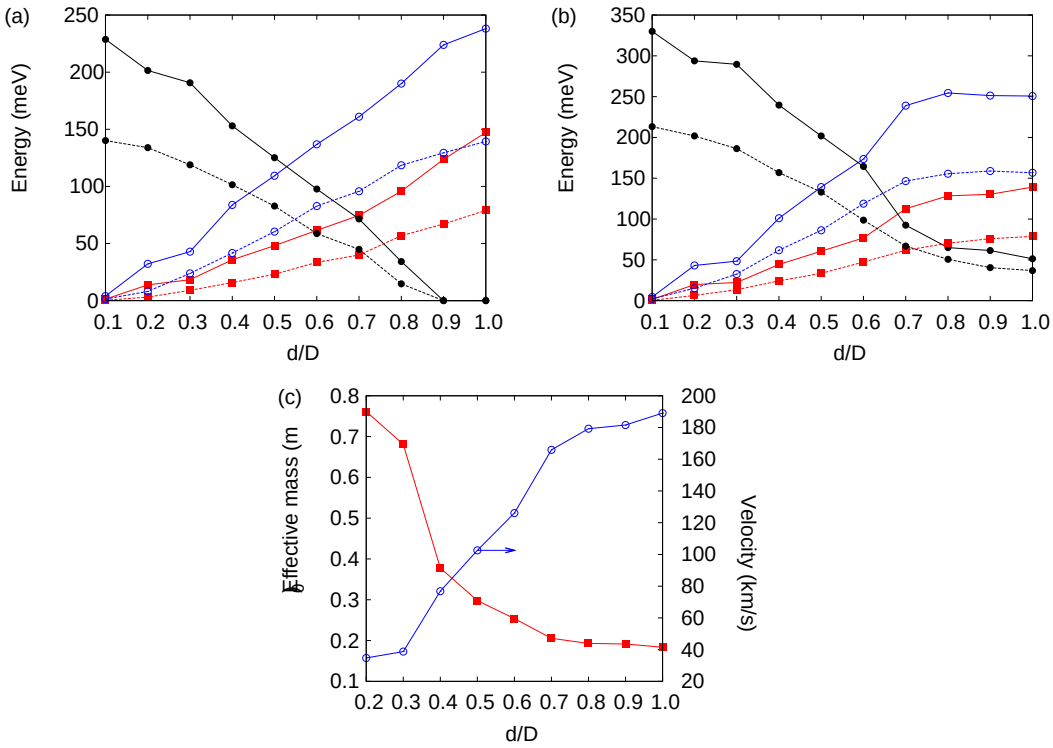

Fig. 3 (a) Total width of the 1*S* band (red squares), of the 1*P* band (blue open circles) and of the gap between 1*S* and 1*P* bands (black solid circles) for square lattices (solid lines: $D = 6.0$ nm; dotted lines: $D = 8.5$ nm). (b) Same for honeycomb lattices (solid lines: $D = 4.7$ nm; dotted lines: $D = 6.4$ nm). (c) Effective mass (in units of the free electron mass m_0) at Γ and group velocity at K for the 1*S* band in honeycomb lattices ($D = 4.7$ nm).